Tamás Insperger
Department of Applied Mechanics,
Budapest University of Technology and Economics,
Budapest H-1521,
Hungary

Janez Gradišek
Faculty of Mechanical Engineering,
University of Ljubljana,
SI-1000 Ljubljana,
Slovenia

Martin Kalveram
Department of Mining Technology,
University of Dortmund,
D-44227 Dortmund,
Germany

Gábor Stépán
Department of Applied Mechanics,
Budapest University of Technology and Economics,
Budapest H-1521,
Hungary

Klaus Winert
Department of Machining Technology,
University of Dortmund,
D-44227 Dortmund,
Germany

Edvard Govekar
Faculty of Mechanical Engineering,
University of Ljubljana,
SI-1000 Ljubljana,
Slovenia

Machine Tool Chatter and Surface Location Error in Milling Processes

A two degree of freedom model of the milling process is investigated. The governing equation of motion is decomposed into two parts: an ordinary differential equation describing the periodic chatter-free motion of the tool and a delay-differential equation describing chatter. The stability chart is derived by using the semi-discretization method for the delay-differential equation corresponding to the chatter motion. The periodic chatter-free motion of the tool and the associated surface location error (SLE) are obtained by a conventional solution technique of ordinary differential equations. It is shown that the SLE is large at the spindle speeds where the ratio of the dominant frequency of the tool and the tooth passing frequency is an integer. This phenomenon is explained by the large amplitude of the periodic chatter-free motion of the tool at these resonant spindle speeds. It is shown that large stable depths of cut with a small SLE can still be attained close to the resonant spindle speeds by using the SLE diagrams associated with stability charts. The results are confirmed experimentally on a high-speed milling center. [DOI: 10.1115/1.2280634]

1 Introduction

The rapid development of machining technology during the past decade and the commercialization of reliable high-speed machining systems have driven the need for thorough dynamical investigations of high-speed cutting processes. One important phenomenon that limits the productivity of machining is the development of self-excited vibrations, also known as machine tool chatter. The work of Tlustý et al. [1] and Tobias [2] led to the development of the "stability lobe diagram" that plots the boundary between stable and unstable cuts as a function of spindle speed and depth of cut.

The accurate modeling of the regenerative effect in cutting processes leads to a delay-differential equation (DDE) with a corresponding infinite dimensional state space [3]. In milling processes, parametric excitation also arises due to the repeated entering and exiting teeth of the rotating tool, therefore, the governing equation for milling is a DDE with time periodic coefficients. Closed form stability conditions cannot be given for the general milling case. Usually, numerical simulations [4–9] and, in the last decade, different analytical techniques [10–19] are used to derive stability charts.

Contributed by the Manufacturing Engineering Division of ASME for publication in the JOURNAL OF MANUFACTURING SCIENCE AND ENGINEERING. Manuscript received December 7, 2004; final manuscript received March 8, 2006. Review conducted by W. J. Endres.

Vibrations arise due to the flexible parts in the system, such as the tool, spindle, workpiece, etc. For some simple cases, when a well defined first mode is dominant, like milling a thin walled workpiece with a stiff mill, the assumption of a single degree of freedom (DOF) model is satisfactory. In this case, the stability chart consists of an infinite series of stability lobes that are associated with either secondary Hopf or period doubling (flip) bifurcations. The analysis of the vibration frequencies [20] and the chatter signal [21] resulted in a thorough understanding of the 1 DOF case.

Usually, there is no single well defined dominant mode of the tool-workpiece system, and the process must be modeled as a multi-DOF one (see, e.g, Refs. [6,22]). One example is when the tool is the most flexible part, and it is modeled as a cantilever beam [23]. In this case, a 2 DOF model is considered with the symmetric parameters in the x and y directions and diagonal modal matrices arise in the equation of motion.

If further modes also play an important role in the system's dynamics, then the stability charts are even more complicated. For these cases, the estimation of the modal parameters requires a sophisticated modal analysis of the combined structure—the tool, the tool holder, and the workpiece [24,25].

The positional accuracy of the milled surface is influenced by the process dynamics. Due to the relative vibrations between the tool and the workpiece, the location of finished surface differs from the desired one left by a perfectly rigid tool on a perfectly

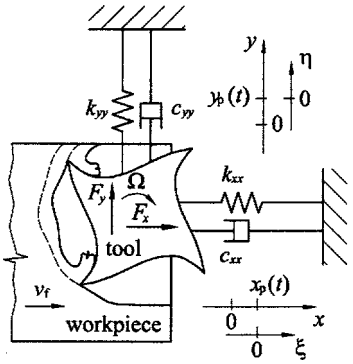

Fig. 1 Schematic mechanical model of the milling process

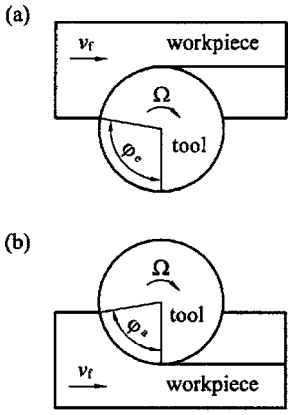

Fig. 2 Schematic of down-milling (*a*) and up-milling (*b*)

rigid workpiece. In the literature, the difference between the desired surface and the actual surface due to the tool and the workpiece compliances is called the surface location error (SLE) [26–32]. Note that other error sources, such as geometric errors in the machine axis or thermal errors, also play an important role in the accuracy of the machining process but are separate from the notion of surface location error.

Having a small SLE is especially important in finishing operations with small radial immersion, since it determines the accuracy of the workpiece's final dimension. Usually, small depths of cut are used to avoid undesired vibrations and inaccuracies of the final product. Therefore, finishing operations usually takes a considerable part of the duration of the whole machining process. An increase of material removal rate in finishing operations would significantly decrease the machining time. This needs a thorough optimization of the technological parameters with respect to material removal rate (axial depth of cut) and the SLE.

SLE diagrams accompanied by stability charts can effectively help in the design of the machining process. As a first investigation in this direction, simultaneous stability and SLE prediction were performed using the time finite element method by Mann et al. [31,32].

In this paper, a 2 DOF model of the milling process is investigated. The governing equation of motion is decomposed into two parts: an ordinary differential equation describing the periodic chatter-free motion of the tool and a delay-differential equation describing chatter. Stability charts are derived by using the semi-discretization method [33,34] for the delay-differential equation corresponding to the chatter motion. The periodic chatter-free motion of the tool and the associated SLE are obtained by a conventional solution technique of ordinary differential equations. It is shown that the SLE is large at the spindle speeds where the ratio of the dominant frequency of the tool and the tooth passing frequency is integer. This phenomenon is explained by the large amplitude of the periodic chatter-free motion of the tool at these resonant spindle speeds. It is shown that large stable depths of cut with a small SLE can still be attained close to the resonant spindle speeds by using SLE diagrams accompanied by stability charts. The results are confirmed experimentally on a high-speed milling center.

2 Mechanical Model

The standard 2 DOF mechanical model of end milling is shown in Fig. 1. The tool is assumed to be flexible relative to the rigid workpiece. The 2 DOF oscillator is excited by the cutting force $\mathbf{F}(t)$. The governing equation has the form

$$\mathbf{M}\ddot{\mathbf{x}}(t) + \mathbf{C}\dot{\mathbf{x}}(t) + \mathbf{K}\mathbf{x}(t) = \mathbf{F}(t) \tag{1}$$

where

$$\mathbf{x}(t) = \begin{bmatrix} x(t) \\ y(t) \end{bmatrix}, \quad \mathbf{F}(t) = \begin{bmatrix} F_x(t) \\ F_y(t) \end{bmatrix}$$

and $\mathbf{M}$, $\mathbf{C}$, and $\mathbf{K}$ are the modal mass, damping, and stiffness matrices, respectively. If the tool is modeled as a symmetric beam, its modal matrices are diagonal with the same diagonal values. In practice, however, the tool is not perfectly symmetric due to the helical flutes, and the modal matrices are not diagonal. In this case, an accurate modeling results in time periodic modal matrices due to the rotation of the flexible tool. However, the tool can usually be considered almost symmetric and the cross terms in the modal matrices can be neglected.

The tangential and the normal forces acting on jth tooth are

$$F_{jt}(t) = g[\varphi_j(t)]K_t a_p h(t) \tag{2}$$

$$F_{jn}(t) = g[\varphi_j(t)]K_n a_p h(t) \tag{3}$$

where K_t and K_n are the linear tangential and the linear normal cutting coefficients, respectively, a_p is the axial depth of cut, and $h(t)$ is the instantaneous chip thickness. For a tool with N evenly spaced teeth, the angular position of the jth cutting edge is

$$\varphi_j(t) = \frac{2\pi\Omega}{60}t + \frac{2\pi(j-1)}{N} \tag{4}$$

where Ω is the spindle speed in revolutions per minute (rpm). The function $g[\varphi_j(t)]$ is a screen function, it is equal to 1 or 0 if the jth tooth is cutting or not

$$g[\varphi_j(t)] = \begin{cases} 1 & \text{if } \varphi_e < \varphi_j(t) < \varphi_a \\ 0 & \text{otherwise} \end{cases} \tag{5}$$

where φ_e and φ_a are the angles where the jth tooth enters and exits the cut, respectively. For down-milling operation, $\varphi_a = \pi$, for up-milling, $\varphi_e = 0$ (see Fig. 2). Note that the entry and exit angles may vary due to heavy vibrations of the tool. This effect is neglected here, and the angles φ_e and φ_a are approximated by constant values as it is usually done in the literature.

The x and y components of the cutting force are given as (see Fig. 3)

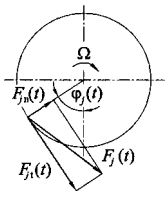

Fig. 3 Cutting force model

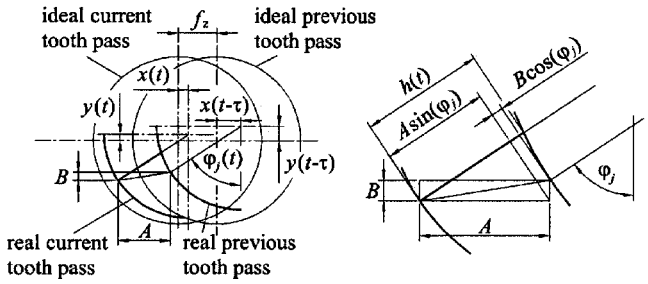

Fig. 4 Chip thickness model

$$F_{jx}(t) = F_{jt}(t)\cos\varphi_j(t) + F_{jn}(t)\sin\varphi_j(t) \tag{6}$$

$$F_{jy}(t) = -F_{jt}(t)\sin\varphi_j(t) + F_{jn}(t)\cos\varphi_j(t) \tag{7}$$

Let the feed per tooth be denoted by $f_z = v_f\tau$, where v_f is the feed speed and $\tau = 60/(N\Omega)$ is the tooth passing period. If $f_z \ll R$, where R is the radius of the tool, then the instantaneous chip thickness can be expressed according to Fig. 4 as

$$h(t) \approx A\sin\varphi_j(t) + B\cos\varphi_j(t) = [f_z + x(t-\tau) - x(t)]\sin\varphi_j(t) + [y(t-\tau) - y(t)]\cos\varphi_j(t) \tag{8}$$

In Fig. 4, the ideal tooth pass is associated with the motion of the teeth of an ideally rigid tool, while the actual tooth pass is associated with the motion of the teeth of the real flexible tool.

The resultant cutting forces are the sum of the forces acting on the teeth

$$F_x(t) = \sum_{j=1}^{N} F_{jx}(t) = \sum_{j=1}^{N} g[\varphi_j(t)][K_t\cos\varphi_j(t) + K_n\sin\varphi_j(t)]a_p h(t) \tag{9}$$

$$F_y(t) = \sum_{j=1}^{N} F_{jy}(t) = \sum_{j=1}^{N} g[\varphi_j(t)][-K_t\sin\varphi_j(t) + K_n\cos\varphi_j(t)]a_p h(t) \tag{10}$$

Using Eqs. (8)–(10), the equation of motion (1) can be written in the form

$$\mathbf{M}\ddot{\mathbf{x}}(t) + \mathbf{C}\dot{\mathbf{x}}(t) + \mathbf{K}\mathbf{x}(t) = a_p\mathbf{H}(t)[\mathbf{x}(t-\tau) - \mathbf{x}(t)] + \mathbf{G}(t) \tag{11}$$

where the elements of the so-called specific cutting force variation matrix $\mathbf{H}(t)$ are

$$H_{xx}(t) = \sum_{j=1}^{N} g[\varphi_j(t)][K_t\cos\varphi_j(t) + K_n\sin\varphi_j(t)]\sin\varphi_j(t) \tag{12}$$

$$H_{xy}(t) = \sum_{j=1}^{N} g[\varphi_j(t)][K_t\cos\varphi_j(t) + K_n\sin\varphi_j(t)]\cos\varphi_j(t) \tag{13}$$

$$H_{yx}(t) = \sum_{j=1}^{N} g[\varphi_j(t)][-K_t\sin\varphi_j(t) + K_n\cos\varphi_j(t)]\sin\varphi_j(t) \tag{14}$$

$$H_{yy}(t) = \sum_{j=1}^{N} g[\varphi_j(t)][-K_t\sin\varphi_j(t) + K_n\cos\varphi_j(t)]\cos\varphi_j(t) \tag{15}$$

as it was also shown by Altintas and Budak [10], and the elements of the stationary cutting force vector $\mathbf{G}(t)$ are

$$G_x(t) = a_p f_z H_{xx}(t) \tag{16}$$

$$G_y(t) = a_p f_z H_{yx}(t) \tag{17}$$

Note, that $\mathbf{H}(t)$ and $\mathbf{G}(t)$ are τ periodic.

3 Forced and Self-Excited Motions of the Tool

The motion of the workpiece is decomposed in the form

$$\mathbf{x}(t) = \mathbf{x}_p(t) + \boldsymbol{\xi}(t) = \begin{bmatrix} x_p(t) \\ y_p(t) \end{bmatrix} + \begin{bmatrix} \xi(t) \\ \eta(t) \end{bmatrix} \tag{18}$$

where $\mathbf{x}_p(t+\tau) = \mathbf{x}_p(t)$ is the forced periodic chatter free motion of the tool, and $\boldsymbol{\xi}(t)$ is a perturbation corresponding to the self-excited vibrations (chatter) of the tool. Substitution of Eq. (18) into Eq. (11) results in

$$\mathbf{M}\ddot{\boldsymbol{\xi}}(t) + \mathbf{C}\dot{\boldsymbol{\xi}}(t) + \mathbf{K}\boldsymbol{\xi}(t) + \mathbf{M}\ddot{\mathbf{x}}_p(t) + \mathbf{C}\dot{\mathbf{x}}_p(t) + \mathbf{K}\mathbf{x}_p(t) = a_p\mathbf{H}(t)[\boldsymbol{\xi}(t-\tau) - \boldsymbol{\xi}(t)] + \mathbf{G}(t) \tag{19}$$

For the ideal case, when no chatter arises, i.e., $\boldsymbol{\xi}(t) \equiv \mathbf{0}$, and the motion is described by $\mathbf{x}(t) = \mathbf{x}_p(t)$, the corresponding equation of motion is the ordinary differential equation

$$\mathbf{M}\ddot{\mathbf{x}}_p(t) + \mathbf{C}\dot{\mathbf{x}}_p(t) + \mathbf{K}\mathbf{x}_p(t) = \mathbf{G}(t) \tag{20}$$

The assumption in Eq. (18) is appropriate, if Eq. (20) has a τ-periodic solution. Since the excitation $\mathbf{G}(t)$ is τ periodic, the stationary (particular) solution of Eq. (20) is also τ periodic. This validates assumption (18).

For linear stability analysis, the variational system of Eq. (11) is determined around the periodic chatter-free motion $\mathbf{x}_p(t)$. Equations (19) and (20) imply the equation

$$\mathbf{M}\ddot{\boldsymbol{\xi}}(t) + \mathbf{C}\dot{\boldsymbol{\xi}}(t) + \mathbf{K}\boldsymbol{\xi}(t) = a_p\mathbf{H}(t)[\boldsymbol{\xi}(t-\tau) - \boldsymbol{\xi}(t)] \tag{21}$$

If the cutting process is stable, the component $\boldsymbol{\xi}(t)$ corresponding to the chatter signal decays, and the tool moves according to the periodic chatter-free motion described by $\mathbf{x}_p(t)$. If the process is unstable, $\boldsymbol{\xi}(t)$ increases exponentially, and the resultant motion $\mathbf{x}(t) = \mathbf{x}_p(t) + \boldsymbol{\xi}(t)$ will also obtain exponential growth. For unstable machining, the nonlinear phenomena also play an important role in the system's dynamics. Due to its large vibrations, the tool leaves the cut, and the cutting force instantly drops to zero. This nonlinearity actually stops the exponential amplitude growth so that, in practice, the tool vibrations during unstable machining still have a finite amplitude [35]. From manufacturing point of view, these large amplitude motions of the tool are not desired since they affect both the surface quality [36,37] and the SLE [26–32]. The aim is to obtain a chatter-free cutting process corresponding to the motion $\mathbf{x}_p(t)$ with the smallest possible vibration amplitude and SLE. Therefore, in the present study, the linear Eqs. (20) and (21) and the corresponding motions, $\mathbf{x}_p(t)$ and $\boldsymbol{\xi}(t)$ are investigated, and nonlinear phenomena are not considered.

The periodic component $\mathbf{x}_p(t)$ is determined by the stationary solution of the forced linear ordinary differential equation (20). This solution can be constructed by Fourier approximation of the forcing vector $\mathbf{G}(t)$ (see, e.g., Refs. [38–40]) and by using the standard harmonic balance method.

The linear stability of the milling process is described by Eq. (21). The stability analysis of this time periodic DDE can be determined by the semi-discretization method [33,34]. The point of the method is that the delayed terms and the time periodic coefficients of the governing time periodic DDE are discretized, while the actual time domain terms and their derivatives are left in the original form. This approximation provides a series of ordinary differential equations that can be solved in each semi-discretization step. Solution of these equations with matching initial conditions results in a finite dimensional Floquet transition matrix. If the eigenvalues of this matrix are in modulo less than 1,

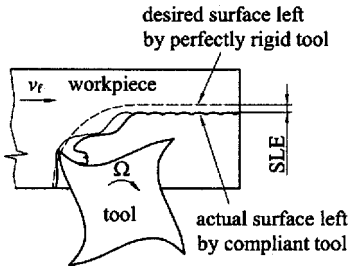

Fig. 5 Surface location error defined by the desired and the actual milled surfaces

then the process is stable, otherwise, it is unstable and chatter arises. In milling processes, two types of instabilities can be observed [20]

1. The eigenvalue is complex, and its magnitude is larger than 1. This case corresponds to secondary Hopf bifurcation and quasi-periodic chatter arises.
2. The eigenvalue is real, and it is smaller than −1. This case corresponds to period doubling or flip bifurcation, and periodic chatter arises.

Stability charts can be created by computing the critical eigenvalues for a set of fixed spindle speeds and depths of cut. The detailed method with the computation code for constructing stability charts for a 2 DOF milling process can be found in Ref. [34].

4 Surface Location Error

SLE is the positional difference between the desired surface left by a perfectly rigid tool and the actual surface left by a compliant tool as shown in Fig. 5.

For the ideal case, when the tool is rigid and no vibrations arise, the path of the jth tooth is described by the combination of the tool rotation and the feed motion $v_f t$

$$\mathbf{x}_{\mathrm{id},j}(t)=\begin{bmatrix} x_{\mathrm{id},j}(t) \\ y_{\mathrm{id}},j(t) \end{bmatrix}=\left\{\begin{matrix} -R\sin\left[\dfrac{(j-1)2\pi}{N}+\dfrac{2\pi\Omega}{60}t\right] \\ -R\cos\left[\dfrac{(j-1)2\pi}{N}+\dfrac{2\pi\Omega}{60}t\right] \end{matrix}\right\}+\begin{pmatrix} v_f t \\ 0 \end{pmatrix} \tag{22}$$

where R is the radius of the tool. Due to the flexibility of the tool, the actual paths of the teeth are affected by the vibrations of the tool. If the cutting process is stable (i.e., $\boldsymbol{\xi}(t)=0$), then the actual path of the jth tooth is

$$\mathbf{x}_j(t)=\begin{bmatrix} x_j(t) \\ y_j(t) \end{bmatrix}=\mathbf{x}_{\mathrm{id},j}(t)+\mathbf{x}_{\mathrm{p}}(t)=\begin{bmatrix} x_{\mathrm{id},j}(t) \\ y_{\mathrm{id},j}(t) \end{bmatrix}+\begin{bmatrix} x_{\mathrm{p}}(t) \\ y_{\mathrm{p}}(t) \end{bmatrix} \tag{23}$$

SLE is the signed difference between the desired surface and the actual surface

$$\mathrm{SLE}=q\left\{\max_t[y_{\mathrm{id},j}(t)]-\max_t[y_j(t)]\right\} \tag{24}$$

where, for down-milling operations, $q=1$, for up-milling, $q=-1$ (see Fig. 6). If the tool cuts deeper than commanded, then the SLE is negative, if the tool cuts shallower than commanded, then the SLE is positive. Negative SLE might sound strange since one would think that the deflections of the tool points always away from the workpiece. However, the tool's deflection should be considered in time, and it can be seen that for some spindle speed domains, heavy vibrations of the tool may result in a negative SLE. In the case of a positive SLE, the accuracy of the workpiece can be improved by additional material removal operations, while in the case of a negative SLE, the error cannot be corrected this way. In this sense, a negative SLE is more unfavorable than a positive SLE.

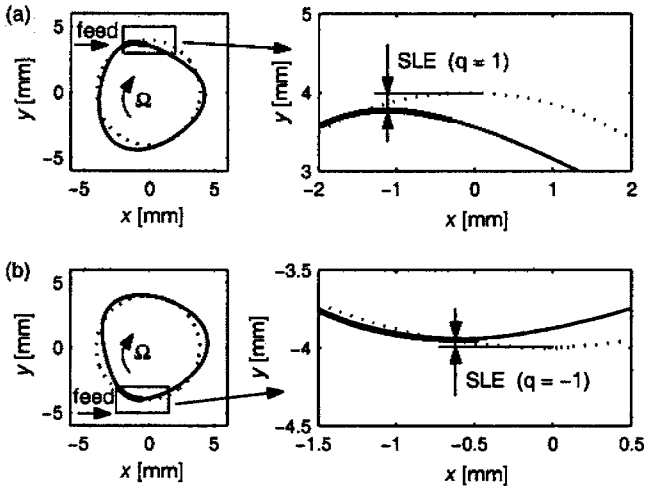

Fig. 6 Tooth path for 10% immersion down-milling (*a*) and 10% immersion up-milling (*b*). Dotted lines denote the desired tooth pass, continuous lines denote the actual tooth pass. Thick lines denote contact of the tool and the workpiece, thin lines denote free oscillation of the tool.

An example for the actual and the desired tooth pass and the associated SLE is shown in Fig. 6. It can be seen that the periodic chatter-free motion of the tool superimposes on the ideal tooth pass that causes error in the surface location.

Note, that expression (24) is valid only for stable cutting processes. For an unstable process, the chatter motion $\boldsymbol{\xi}(t)$ should also be incorporated. However, since unstable cutting process is not a desired way of manufacturing, here, only the stable machining case is investigated.

5 Stability Chart and SLE Diagrams

Theoretical and experimental stability charts and surface location errors for 10% immersion down-milling can be seen in Fig. 7. Theoretical stability chart was determined using the semi-discretization technique according to Ref. [34]. The experimental chart was obtained by cutting tests conducted at a series of spindle speeds and cutting depths. Tool deflections were measured during cutting in the x and y directions simultaneously by a couple of laser optical displacement sensors mounted on the spindle housing. Stability of the cutting tests was assessed based on the recorded tool deflections, sound emitted during cutting, and roughness of the machined surface. The tests were performed on a high speed milling center using an 8 mm diameter end mill with a single cutting edge ($N=1$). Originally, the cutter had two teeth but one tooth was ground off in order to avoid disturbances due to the runout. The feed per tooth was $f_z=0.16$ mm. The workpiece was a square block made of $AlMgSi_{0.5}$ aluminum alloy, for which the cutting force coefficients were determined mechanistically [41]: $K_t=644\times10^6$ N/m^2, $K_n=237\times10^6$ N/m^2. During the experiments, minimal amount of coolant was used.

The modal parameters were determined by standard impact test procedure [42]. The modal matrices are

$$\mathbf{M}=\begin{pmatrix} 0.0199 & 0 \\ 0 & 0.0201 \end{pmatrix}\mathrm{kg}$$

$$\mathbf{C}=\begin{pmatrix} 1.603 & 0 \\ 0 & 1.557 \end{pmatrix}\mathrm{Ns/m}$$

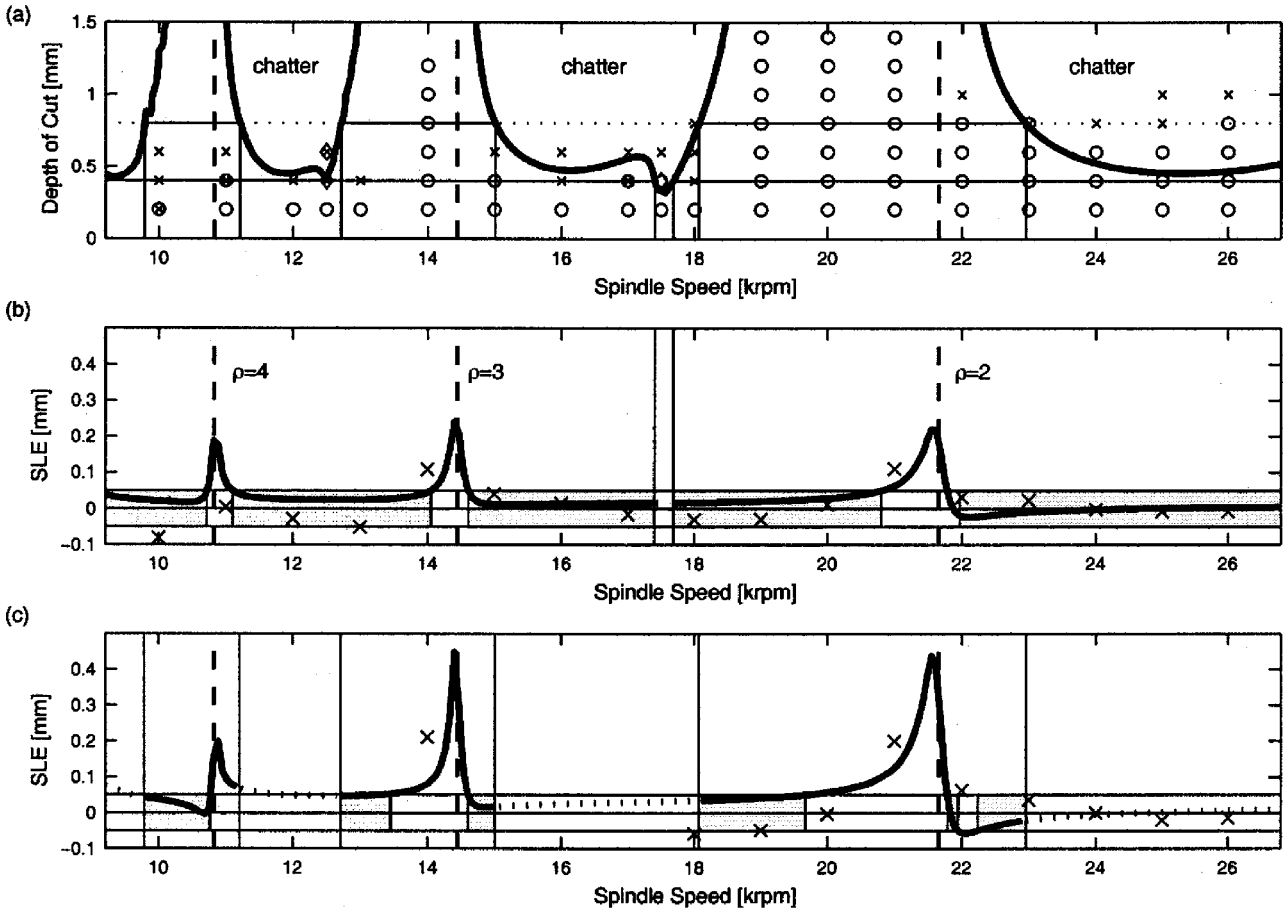

Fig. 7 (*a*) **Theoretical and experimental stability chart for 10% immersion down-milling. Thick lines denote theoretical stability boundary, circles denote stable cutting, crosses denote quasi-periodic chatter, diamonds denote period doubling chatter.** (*b*), (*c*) **Theoretical and experimental surface location errors for a_p=0.4 mm** (*b*) **and a_p=0.8 mm** (*c*). **Dotted lines denote the theoretical SLE for unstable cutting, continuous lines denote the theoretical SLE for stable cutting, crosses denote the experimental SLE.**

$$\mathbf{K} = \begin{pmatrix} 409000 & 0 \\ 0 & 413000 \end{pmatrix} \text{N/m}$$

More details on the experiments and on the identification of the system parameters can be found in Refs. [41,42].

In spite of some small quantitative discrepancies, experimental and theoretical charts agree well especially for spindle speeds 12–26 krpm. There might be several possible reasons for the small differences. At small depths of cut, any contact between the tool and the workpiece may cause differences. The entry and exit angles may vary due to the tool vibrations and they are not constant as it is assumed in Eq. (5). The traditional chip thickness model in Eq. (8) looses accuracy for low radial immersion (see, e.g., Refs. [43,44]). The values of the cutting force coefficients may also vary for different spindle speeds (the values used here were determined at constant spindle speed 4000 rpm). Experiments have also showed that the dominant frequency of the tool decreases as spindle speed is increased (see Ref. [42]). However, in spite of the approximations in the model, it should be emphasized that the experimental and theoretical results agree well in the presented parameter domains.

Introduce the frequency ratio $\rho = f_t / f_{tpe}$, where $f_t \approx f_x \approx f_y \approx 722$ Hz is the natural frequency of the tool and $f_{tpe} = N\Omega/60$ is the tooth pass excitation frequency. Note that frequency ratio is the inverse of the normalized spindle speed that is usually used in the machine tool vibration literature. If ρ is close to an integer, then the forced system (20) is close to resonance, i.e. the first or the higher harmonics of the cutting force variation excite the first mode of the tool. The dashed vertical lines at 10.8, 14.4, and 21.7 krpm in Fig. 7 denote these resonant spindle speeds corresponding to ρ=2, 3, and 4, respectively. As it can be seen, large depth of cut values can be achieved without chatter around these resonant spindle speeds.

Theoretical surface location error was determined using Eqs. (22)–(24) for two depths of cut: a_p=0.4 and 0.8 mm. These depth of cut values are also shown in the stability chart in panel (*a*) of Fig. 7: the parameters corresponding to stable and unstable machining are denoted by continuous and dotted horizontal lines, respectively. Experimental SLE was computed from the measured tool deflection data. This cannot be considered as a pure experimental result, but this gives a good estimation of the real experimental SLE as it was shown in Refs. [31,32].

In panels (*b*) and (*c*) of Fig. 7, the theoretically predicted SLE correlates well with the experimental one. As it can be seen, the SLE is especially large at the resonant spindle speeds, where ρ is close to integer. This phenomenon can be explained by the periodic component $\mathbf{x}_p$ of the tool motion. If ρ is close to integer, then the forced system (20) is close to resonance, and the amplitude of the periodic component $\mathbf{x}_p$ is large. This affects the position of cutting edges during cutting, and, consequently, influences the SLE.

Figure 8 shows theoretical trajectory of the tool at spindle speeds 14–21 krpm with axial depth of cut a_p=0.4 mm. This series of plots can be associated with panel (*b*) in Fig. 7. It can be seen that the vibration amplitudes are large at 14 and 21 krpm that

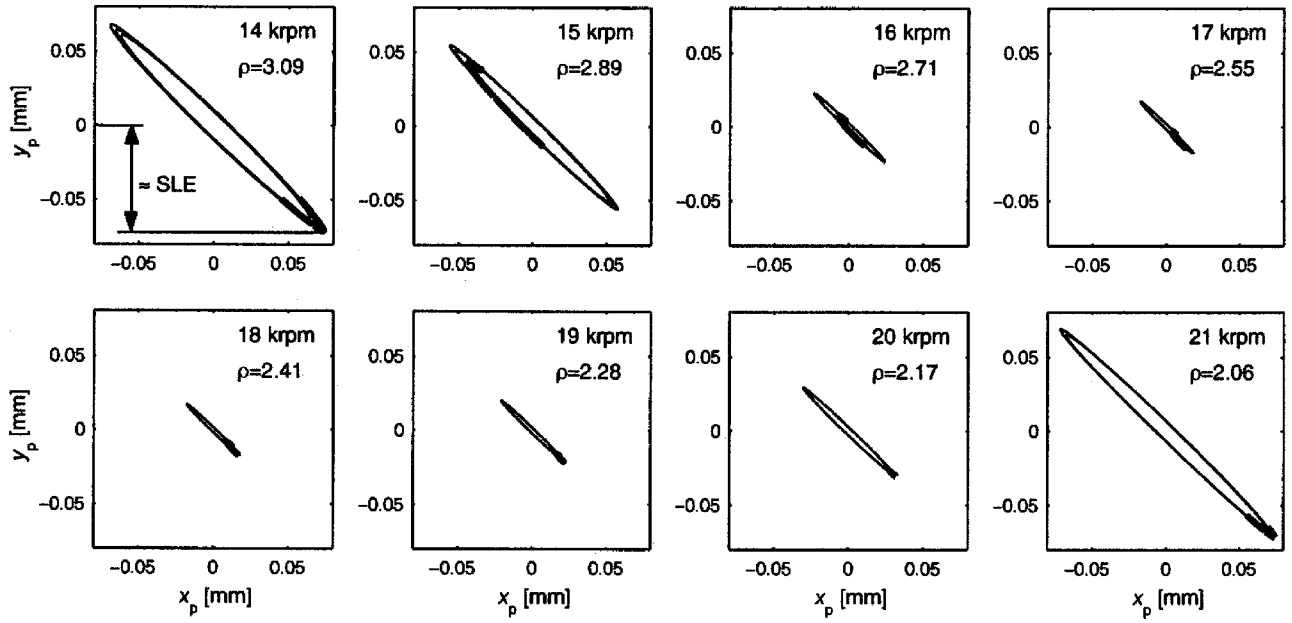

Fig. 8 Theoretical periodic chatter-free tool trajectories for 10% immersion down-milling with a_p=0.4 mm and different spindle speeds. Thick lines denote contact of the tool and the workpiece, thin lines denote free oscillation of the tool.

are close to the resonant spindle speeds with ρ=3 and 2, respectively, while the vibration amplitudes are smaller at the spindle speeds between 14 and 21 krpm. The origin of the plane (x_p, y_p) corresponds to zero SLE produced by the ideally rigid tool, while the real surface is modulated according to the path of the compliant tool. Consequently, SLE is approximately equal to the maximal deflection of the tool in the y direction during cutting (see case 14 krpm in Fig. 8). This series of plots gives a clear explanation for a large SLE close to the resonant spindle speeds.

Another interesting feature of the tool trajectories are the number of cycles in the plane (x,y) completed by the tool during a tooth pass. At spindle speed 14 krpm, f_{tpe}=233.3 Hz, the frequency ratio is $\rho=f_t/f_{tpe}=3.09\approx3$, and the tool oscillates about three cycles during a tooth pass. For spindle speeds 15–20 krpm, ρ decreases from 2.89 to 2.17, and one of the cycles gets smaller and smaller and slowly disappears. At 21 krpm, ρ=2.07 and the tool clearly makes two cycles during a tooth pass. This shows that the frequency ratio approximately characterizes the number of cycles completed by the tool in the plane (x,y) during a tooth pass. For example, at 17 krpm, ρ=2.55, and the tool makes two large cycles of about the same amplitude corresponding to free oscillation of the tool (thin line) and a smaller cycle corresponding to contact between the tool and the workpiece (thick line), so the number of cycles can be said to be about 2 1/2.

Figure 9 shows the theoretical and the experimental tool trajectory corresponding to the resonant spindle speeds 14 and 21 krpm. The noise-free experimental trajectories were obtained by a nonlinear filtering technique suitable for periodically forced processes [21]. The experimental plots clearly show that at spindle speeds 14 and 21 krpm, the tool completes two and three cycles, indeed.

6 Selection of Optimal Spindle Speed

During the selection of spindle speeds, both the stability chart and the SLE diagram should be considered. Optimal spindle speeds allow large depth of cut with stable machining and result in a small SLE at the same time. Since the SLE is large at the lines ρ=integer, spindle speed should be chosen carefully either to the left or to the right to these lines but still within the stable domain. Note that the stable domains to the left to this resonant lines are wider than the ones to the right. For example, consider the case $\rho\approx2$ and a_p=0.8 mm in Fig. 7. In this case, the stable spindle speeds are between 18.1 and 23.0 krpm and the resonant spindle speed is 21.7 krpm. The width of stable spindle speed range to the left to the line ρ=2 is 21.7−18.1=3.6 krpm, while to the right, it is 23.0−21.7=1.3 krpm. The wider the suitable parameter range, the more robust the system against disturbances. In the given case, the optimal spindle speed is suggested to be chosen in the domain 18.1–21.7 krpm.

In panels (*b*) and (*c*) in Fig. 7, gray color denotes the optimal

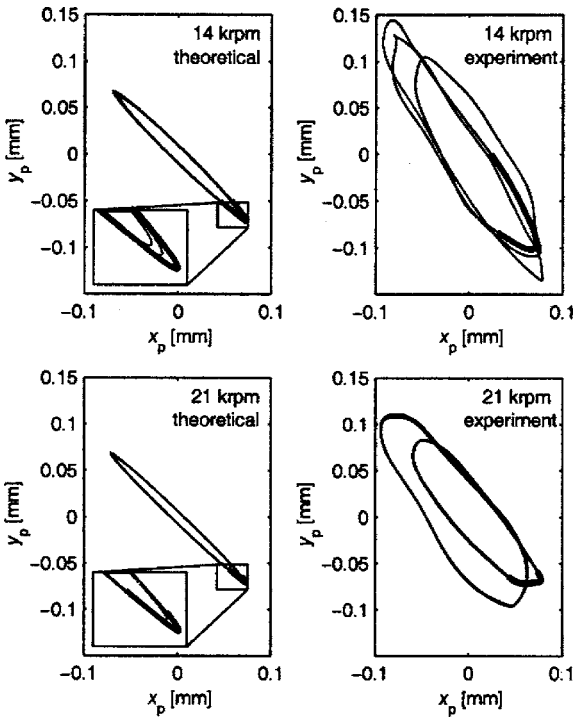

Fig. 9 Theoretical and experimental tool trajectories for 10% immersion down-milling with a_p=0.4 mm. Thick lines denote contact of the tool and the workpiece, thin lines denote free oscillation of the tool.

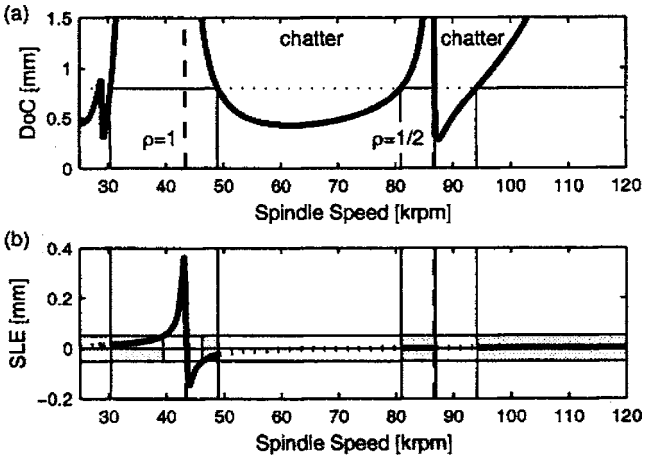

Fig. 10 (*a*) Theoretical stability chart for 10% immersion down-milling in the high-speed domain. (*b*) Theoretical surface location error for a_p=0.8 mm.

spindle speed domains that result in a SLE less than 0.05 mm with stable machining. It can be seen that the optimal domains are wider to the left to the resonant lines than the ones to the right.

Another aspect in the selection of spindle speed is the sign of the resulted SLE. As it was mentioned earlier, a positive SLE is less unfavorable than a negative SLE, since in the case of a positive SLE, the accuracy of the workpiece can be improved by additional material removal operations, while in the case of a negative SLE, the error cannot be corrected this way. In Fig. 7, it can be seen that the spindle speeds to the right to the resonant lines may result in a negative SLE, while the domains to the left result in a positive SLE. This point also support the choice of spindle speeds to the left to the resonant lines.

A general structural feature of milling stability charts is that stable areas are usually wider at higher resonant spindle speeds. It can also be seen in Fig. 7 that stable spindle speed regions are wider for smaller ρ. For example, the width of stable spindle speed domains at a_p=0.8 mm are 11.2−9.8=1.4 krpm at $\rho\approx4$, 15.0−12.7=2.3 krpm at $\rho\approx3$, and 23.0−18.1=4.9 krpm at $\rho\approx2$. This shows that it is easier to find an optimal spindle speed with a small SLE in the high-speed domain than in the low-speed one.

Figure 10 shows the stability chart and the corresponding SLE diagram for spindle speeds close to the natural frequency of the tool and above. The spindle speeds associated with $\rho=1$ and $\rho=1/2$ (43.3 and 86.6 krpm, respectively) are denoted by dashed lines and grey color denotes the optimal spindle speeds that result in a SLE less than 0.05 mm. Note that the stability lobe between the lines $\rho=1$ and $\rho=1/2$ is the first Hopf lobe, and the lobe to the right to the line $\rho=1/2$ is the first period doubling (flip) lobe, i.e., there are no more additional stability boundaries for spindle speeds larger than 110 krpm. The location of the optimal spindle speeds around the line $\rho=1$ is similar to those of at $\rho=2$, 3, and 4, but the regions are wider: the one to the left to the line $\rho=1$ is of width 39.4−30.3=9.1 krpm. If the system is operated close to the line $\rho=1/2$, then two optimal domains are obtained. The one below the line $\rho=1/2$ is of width 86.8−80.9=5.9 krpm, the other starts at about 94 krpm and goes theoretically to infinity. This implies that operating the system at higher speeds than twice the first resonant spindle speed results in both stable machining with a large depth of cut and a small SLE. Note, however, that at these extremely high spindle speeds, the higher modes of the machine-tool-workpiece structure that were neglected in this approach may become important and may destroy this clear structure shown in Fig. 10.

7 Conclusions

Stability, tool motion, and surface location error were investigated for a 2 DOF milling process. A mechanical model including both the regenerative and the tooth pass excitation effect was used to derive the equation of motion. The vibration of the tool was decomposed into a periodic chatter-free motion and the chatter motion. The periodic chatter-free motion is described by an ordinary differential equation, while the chatter motion is described by a time periodic delay-differential equation. For unstable machining, the unstable chatter motion is superimposed on the chatter-free periodic motion. Stability diagrams were obtained by using the numerical semi-discretization method for the DDE of chatter. The periodic chatter-free motion corresponding to stable machining was determined by solving the governing ordinary differential equation with excitation. By considering the tool rotation and the feed motion, the position of the cutting edges and, consequently, the location of the resulted surface on the workpiece can be computed. The surface location error (the difference between the commanded surface and the machined surface) was determined and accompanied by the stability chart. It was pointed out that the sign of the SLE might also be important, since a positive SLE can be corrected by additional operations, while a negative SLE cannot.

The ratio of the natural frequency of the tool and the tooth pass excitation frequency ($\rho=f_t/f_{tpe}$) was used to characterize different spindle speed cases. It was shown that a SLE is relatively large at the resonant spindle speeds where ρ is integer due to the resonance between the cutting force variation and the tool. It was also shown that frequency ratio ρ characterizes the number of cycles completed by the tool during a tooth pass. The theoretical results were supported by experimental tests.

Two main observations help the selection of optimal spindle speeds. First, in order to achieve large depth of cut with stable machining and with a small positive SLE, the stable spindle speed regions to the left to the resonant spindle speeds should be used. Second, in the high-speed domain, the stable spindle speeds are wider, which makes the selection of optimal spindle speed easier.

Acknowledgment

This research was supported in part by the Magyary Zoltán Postdoctoral Fellowship of Foundation for Hungarian Higher Education and Research (T.I.), by the Alexander von Humboldt Foundation (J.G.), and by the Hungarian National Science Foundation under Grant nos. OTKA F047318 (T.I.) and OTKA T043368 (G.S., T.I.).

References

[1] Tlustý, J., Poláček, A., Daněk, C., Špaček, J., 1962, *Selbsterregte Schwingungen an Werkzeugmaschinen*, VEB Verlag Technik, Berlin.
[2] Tobias, S. A., 1965, *Machine Tool Vibration*, Blackie, London.
[3] Stépán, G., 1989, *Retarded Dynamical Systems*, Longman, Harlow.
[4] Smith, S., and Tlustý, J., 1991, "An Overview of Modeling and Simulation of the Milling Process," ASME J. Eng. Ind., **113**, pp. 169–175.
[5] Li, H., and Li, X., 2000, "Modelling and Simulation of Chatter in Milling Using a Predictive Force Model," Int. J. Mach. Tools Manuf., **40**, pp. 2047–2071.
[6] Zhao, M. X., and Balachandran, B., 2001, "Dynamics and Stability of Milling Process," Int. J. Solids Struct., **38**(10–13), pp. 2233–2248.
[7] Campomanes, M. L., and Altintas, Y., 2003, "An Improved Time Domain Simulation for Dynamic Milling at Small Radial Immersions," ASME J. Manuf. Sci. Eng., **125**(3), pp. 416–422.
[8] Xu, A.-P., Qu, Y.-X., Zhang, D.-W., and Huang, T., 2003, "Simulation and Experimental Investigation of the End Milling Process Considering the Cutter Flexibility," Int. J. Mach. Tools Manuf., **43**, pp. 283–292.
[9] Paris, H., Peigné, G., and Mayer, R., 2004, "Surface Shape Prediction in High Speed Milling," Int. J. Mach. Tools Manuf., **44**(15), pp. 1591–1597.
[10] Altintas, Y., and Budak, E., 1995, "Analytical Prediction of Stability Lobes in Milling," CIRP Ann., **44**(1), pp. 357–362.
[11] Tian, J., and Hutton, S. G., 2001, "Chatter Instability in Milling Systems With Flexible Rotating Spindles—A New Theoretical Approach," ASME J. Manuf. Sci. Eng., **123**(1), pp. 1–9.
[12] Davies, M. A., Pratt, J. R., Dutterer, B., and Burns, T. J., 2002, "Stability Prediction for Low Radial Immersion Milling," ASME J. Manuf. Sci. Eng., **124**(2), pp. 217–225.

[13] Bayly, P. V., Halley, J. E., Mann, B. P., and Davies, M. A., 2003, "Stability of Interrupted Cutting by Temporal Finite Element Analysis," ASME J. Manuf. Sci. Eng., **125**(2), pp. 220–225.
[14] Faassen, R. P. H., van de Wouw, N., Oosterling, J. A. J., and Nijmeijer, H., 2003, "Prediction of Regenerative Chatter by Modeling and Analysis of High-Speed Milling," Int. J. Mach. Tools Manuf., **43**(14), pp. 1437–1446.
[15] Insperger, T., Mann, B. P., Stépán, G., and Bayly, P. V., 2003, "Stability of Up-Milling and Down-Milling, Part 1: Alternative Analytical Methods," Int. J. Mach. Tools Manuf., **43**(1), pp. 25–34.
[16] Szalai, R., and Stépán, G., 2003, "Stability Boundaries of High-Speed Milling Corresponding to Period Doubling Are Essentially Closed Curves," *Proceedings of ASME International Mechanical Engineering Conference and Exposition*, Washington, DC, Paper No. IMECE2003-42122 (CD-ROM).
[17] Wang, J.-J. J., Zheng, C. M., and Huang, C. Y., 2003, The Effect of Harmonic Force Components on Regenerative Stability in End Milling," *Proceedings of the 2003 ASME International Mechanical Engineering Congress and Exposition, Washington, DC*, Paper No. IMECE2003-42367 (CD-ROM).
[18] Merdol, S. D., and Altintas, Y., 2004, "Multi Frequency Solution of Chatter Stability for Low Immersion Milling, ASME J. Manuf. Sci. Eng., **126**(3), pp. 459–466.
[19] Corpus, W. T., and Endres, W. J., 2004, "Added Stability Lobes in Machining Processes That Exhibit Periodic Time Variation—Part 1: An Analytical Solution," ASME J. Manuf. Sci. Eng., **126**(3), pp. 467–474.
[20] Insperger, T., Stépán, G., Bayly, P. V., and Mann, B. P., 2003, "Multiple Chatter Frequencies in Milling Processes," J. Sound Vib., **262**(2), pp. 333–345.
[21] Gradišek, J., Friedrich, R., Govekar, E., and Grabec, I., 2002, "Analysis of Data From Periodically Forced Stochastic Processes," Phys. Lett. A, **294**(3–4), pp. 234–238.
[22] Bravo, U., Altuzarra, O., López de Lacalle, L. N., Sánchez, J. A., and Campa, F. J., 2005, "Stability Limits of Milling Considering the Flexibility of the Workpiece and the Machine," Int. J. Mach. Tools Manuf., **45**, pp. 1669–1680.
[23] Kivanc, E. B., and Budak, E., 2004, "Structural Modeling of End Mills for Form Error and Stability Analysis," Int. J. Mach. Tools Manuf., **44**(11), pp. 1151–1161.
[24] Schmitz, T. L., Davies, M. A., and Kennedy, M. D., 2001, "Tool Point Frequency Response Prediction for High-Speed Machining by RCSA," ASME J. Manuf. Sci. Eng., **123**(4), pp. 700–707.
[25] Young, K. A., and Helvey, A. M., 2003, "Requirements for Consistent and Productive Performance in High Speed Milling," *Proceedings of the 2003 ASME International Mechanical Engineering Congress and Exposition*, Washington, DC, Paper No. IMECE2003-41694 (CD-ROM).
[26] Kline, W. A., Devor, R. E., and Shareef, I., 1982, "Prediction of Surface Accuracy in End Milling, ASME J. Eng. Ind., **104**, pp. 272–278.
[27] Sutherland, J. W., and DeVor, R. E., 1986, "An Improved Method for Cutting Force and Surface Error Prediction in Flexible End Milling Systems, ASME J. Eng. Ind., **108**, pp. 269–279.
[28] Montgomery, D., and Altintas, Y., 1991, "Mechanism of Cutting Force and Surface Generation in Dynamic Milling," ASME J. Eng. Ind., **113**, pp. 160–168.
[29] Shirase, K., and Altintas, Y., 1996, "Cutting Force and Dimensional Surface Error Generation in Peripheral Milling With Variable Pitch Helical End Mills," Int. J. Mach. Tools Manuf., **36**(5), pp. 567–584.
[30] Schmitz, T., and Ziegert, J., 1999, "Examination of Surface Location Error Due to Phasing of Cutter Vibrations," Precis. Eng., **23**, pp. 51–62.
[31] Mann, B. P., Bayly, P. V., Davies, M. A., and Halley, J. E., 2004, "Limit Cycles, Bifurcations, and Accuracy of the Milling Process," J. Sound Vib., **277**(1–2), pp. 31–48.
[32] Mann, B. P., Young, K. A., Schmitz, T. L., and Dilley, D. N., 2005, "Simultaneous Stability and Surface Location Error Predictions in Milling," ASME J. Manuf. Sci. Eng., **127**(3), pp. 446–453.
[33] Insperger, T., and Stépán, G., 2002, "Semi-Discretization Method for Delayed Systems," Int. J. Numer. Methods Eng., **55**(5), pp. 503–518.
[34] Insperger, T., and Stépán, G., 2004, "Updated Semi-Discretization Method for Periodic Delay-Differential Equations With Discrete Delay," Int. J. Numer. Methods Eng., **61**(1), pp. 117–141.
[35] Stépán, G., Szalai, R., Mann, B. P., Bayly, P. V., Insperger, T., Gradišek, J., and Govekar, E., 2005, "Nonlinear Dynamics of High-Speed Milling—Analyses, Numerics and Experiments," ASME J. Vibr. Acoust., **127**(2), pp. 197–203.
[36] Lipski, J., Litak, G., Rusinek, R., Szabelski, K., Teter, A., Warmiński, J., and Zaleski, K., 2002, "Surface Quality of a Work Material's Influence on the Vibrations of the Cutting Process," J. Sound Vib., **252**(4), pp. 729–737.
[37] Peigne, G., Paris, H., Brissaud, D., and Gouskov, A., 2004, "Impact of the Cutting Dynamics of Small Radial Immersion Milling Operations on Machined Surface Roughness, Int. J. Mach. Tools Manuf., **44**(11), pp. 1133–1142.
[38] Lazoglu, I., and Liang, S. Y., 1997, "Analytical Modeling of Ball-End Milling Forces," Mach. Sci. Technol., **1**(2), pp. 219–234.
[39] Budak, E., and Altintas, Y., 1998, "Analytical Prediction of Chatter Stability in Milling—Part I: General Formulation," ASME J. Dyn. Syst., Meas., Control, **120**, pp. 22–30.
[40] Budak, E., and Altintas, Y., 1998, "Analytical Prediction of Chatter Stability in Milling—Part II: Application of the General Formulation to Common Milling Systems," ASME J. Dyn. Syst., Meas., Control, **120**, pp. 31–36.
[41] Gradišek, J., Kalveram, M., and Weinert, K., 2004, "Mechanistic Identification of Specific Force Coefficients for a General End Mill," Int. J. Mach. Tools Manuf., **44**(4), pp. 401–414.
[42] Gradišek, J., Kalveram, M., Insperger, T., Weinert, K., Stépán, G., Govekar, E., and Grabec, I., 2005, "On Stability Prediction for Milling," Int. J. Mach. Tools Manuf., **45**(7–8), pp. 741–991.
[43] Li, H. Z., Liu, K., and Li, X. P., 2001, "A New Method for Determining the Undeformed Chip Thickness in Milling," J. Mater. Process. Technol., **113**, pp. 378–384.
[44] Faassen, R., van de Wouw, N., Oosterling, H., and Nijmeijer, H., 2005, "Updated Tool Path Modelling With Periodic Delay for Chatter Prediction in Milling," *Proceedings of the Fifth EUROMECH Nonlinear Dynamics Conference*, Eindhoven, The Netherlands, pp. 1080–1089.